DOI: 10.1002/chem.200802196

Asymmetrically Substituted Benzene-1,3,5-tricarboxamides: Self-Assembly and Odd–Even Effects in the Solid State and in Dilute Solution

Patrick J. M. Stals, Maarten M. J. Smulders, Rafael Martín-Rapún, Anja R. A. Palmans,* and E. W. Meijer*[a]

Abstract: Asymmetric benzene-1,3,5-tricarboxamides (aBTAs) comprising two *n*-octyl and one chiral methyl–alkyl side chain were synthesised and characterised. The influence of the position and the configuration of the chiral methyl group (methyl at the α, β or γ position) in the aliphatic side chains on the liquid-crystalline properties and the aggregation behaviour of the aBTAs was systematically studied and compared to symmetrical benzene-1,3,5-tricarboxamides (sBTAs). Solid-state characterisation (polarised optical microscopy, IR spectroscopy, X-ray diffraction and differential scanning calorimetry) revealed that all aBTAs show threefold, α-helical-type intermolecular hydrogen bonding between neighbouring molecules and exhibit a columnar hexagonal organisation from room temperature to well above 200 °C. Moving the chiral methyl group closer to the amide group stabilises the liquid-crystalline state, as evidenced by a higher clearing temperature and corresponding enthalpy. The self-assembly of dilute solutions of the aBTAs in methylcyclohexane ($\approx 10^{-5}$ mol L^{-1}) was investigated with circular dichroism (CD) spectroscopy. The sign of the Cotton effect demonstrated a pronounced odd–even effect, whereas the value of the molar ellipticity, $\Delta\varepsilon$, in the aBTAs was independent of the position of the methyl group. Subsequent temperature-dependent CD measurements showed that the aggregation of all aBTAs can quantitatively be described by the nucleation-growth model and that the stability of the aggregates increases when the chiral methyl group is closer to the amide moiety. The results presented herein illustrate that even small changes in the molecular structure of substituted benzene-1,3,5-tricarboxamides affect their solid-state properties and their self-assembly behaviour in dilute solutions.

Keywords: chirality · circular dichroism · liquid crystals · self-assembly · synthesis design

Introduction

Self-assembly has attracted considerable interest in the field of (macro)organic chemistry because it allows for the formation of complex, dynamic systems starting from relatively simple building blocks.[1] In this respect, benzene-1,3,5-tricarboxamides (BTAs) represent a particularly interesting class of compounds because they show well-defined aggregates in the solid state, and in concentrated and dilute solutions (Figure 1). BTA-based compounds have been studied in detail as organogelators,[2] liquid crystals,[3] nucleating agents for isotactic polypropylene[4] and nanostructured materials.[5] These rather simple molecules self-assemble into long, helical columnar aggregates due to threefold α-helical-type intermolecular hydrogen bonding and π–π stacking. The helicity in the columns was unequivocally observed in the solid state by crystal structure elucidation (Figure 1).[6] In dilute apolar solutions, strong Cotton effects were observed when a chiral centre was introduced into the alkyl side chains, showing that the helical structure remains intact upon dilution.[7]

To date, studies relating to the self-assembly of alkyl-substituted BTAs in dilute alkane solutions focussed predominantly on symmetrical derivatives comprising three chiral (*R*)- or (*S*)-3,7-dimethyloctyl side chains (sBTA-*R*/*S*-3Me, Scheme 1) or three achiral *n*-octyl side chains (sBTA-C_8, Scheme 1).[7] A disadvantage of using symmetrical BTAs is that diastereomers are formed when the chiral side chain is not optically pure, which complicates the interpretation of

[a] P. J. M. Stals, M. M. J. Smulders, Dr. R. Martín-Rapún, Dr. A. R. A. Palmans, Prof. Dr. E. W. Meijer
Laboratory of Macromolecular and Organic Chemistry and Institute for Complex Molecular Systems
Eindhoven University of Technology, PO Box 513
5600 MB Eindhoven (The Netherlands)
Fax: (+31) 402-451-036
E-mail: A.Palmans@tue.nl
E.W.Meijer@tue.nl

Supporting information for this article is available on the WWW under http://dx.doi.org/10.1002/chem.200802196.

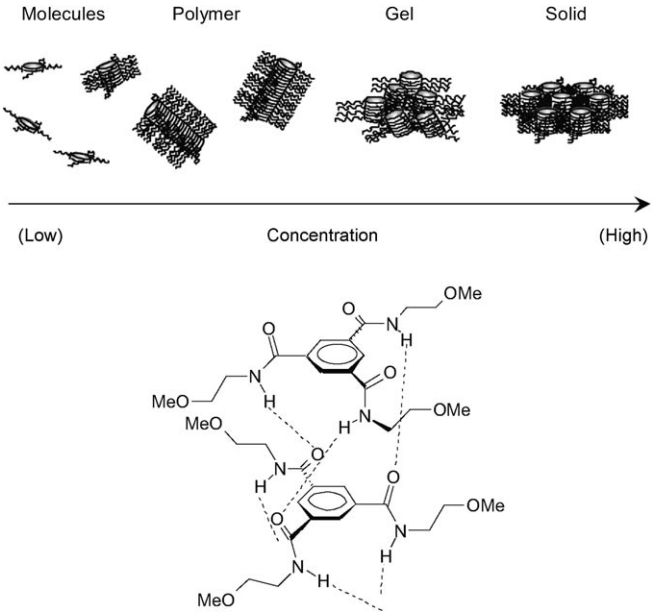

Figure 1. Different aggregation states of BTAs as function of concentration (top) and the helical packing of a BTA derivative in the solid state (bottom).

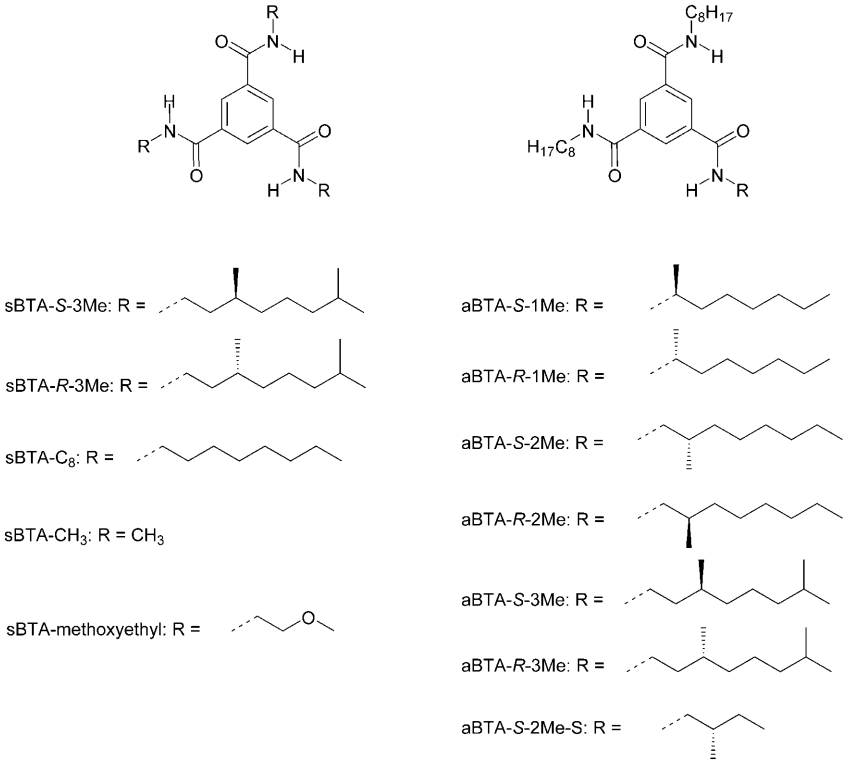

Scheme 1. Chemical structure of symmetric and asymmetric benzene-1,3,5-tricarboxamides (sBTA and aBTA, respectively).

the data. As Hanabusa et al. recently showed, the solution behaviour of *rac*-3,7-dimethyloctyl-substituted BTAs differs significantly from the optically enriched derivatives.[2g] In addition, the solubility of symmetrically α- and β-methyl-substituted derivatives is poor in alkane solvents.[8]

For these reasons, we decided to continue our studies to elucidate the self-assembly of BTAs with asymmetrically substituted BTAs (aBTAs) comprising two achiral, *n*-octyl chains and one chiral chain. Apart from avoiding diastereomeric mixtures, such derivatives allow the systematic study of the effect of changing the configuration and position of one methyl group on the side chain on the solid-state properties and self-assembly behaviour in dilute solutions. In view of odd–even effects observed in (chiral) nematic liquid crystals,[9] helical polymers[10] and helical aggregates of oligo- and polythiophenes,[11] we anticipated that odd–even effects may also be operative in these aBTAs. Typically, the odd–even effect is ascribed to the alteration of the spatial position of a chiral group when moving down an aliphatic chain, which is reflected in the clearing temperatures in nematic liquid crystals, helical pitches in cholesteric mesophases and chiroptical properties of helical polymers and aggregates. For example, when changing the position of a methyl group from the α to the β and γ position along the alkyl chain in helical polyisocyanides and maintaining the same configuration, alternating signs of the Cotton effects were observed.[12]

We herein show the synthesis and characterisation of a new family of aBTAs comprising two *n*-octyl chains. In the third, chiral side chain, we vary the configuration (*R* and *S*) and the position of the methyl group from the α position to the γ position (Scheme 1). Characterisation of the aBTAs in the solid state was conducted with infrared (IR) spectroscopy, differential scanning calorimetry (DSC), polarised optical microscopy (POM) and X-ray diffraction. Two symmetrically substituted reference compounds, sBTA-CH_3[2a] and sBTA-methoxyethyl,[6a] were included in this study because their crystal structures have previously been elucidated. For comparison, we remeasured the solid-state data for selected symmetrically substituted BTAs (sBTAs, sBTA-C_8 and sBTA-*R*/*S*-3Me) under identical conditions. In addition, the self-assembly behaviour in dilute alkane solutions of aBTAs was studied by circular dichroism (CD) spectroscopy to assess the presence of an odd–even effect. CD spectroscopy was recently found to be a powerful tool in elucidating the nature of the self-as-

sembly process in sBTAs.[7b] Finally, temperature-dependent CD measurements were conducted to investigate self-assembly of the aggregates formed and their stability.

Results

Synthesis of asymmetric BTAs: Asymmetric BTAs (aBTAs, Scheme 1) were synthesised by coupling 3,5-bis-*n*-octylaminocarbonyl-benzoic acid[5a] to the appropriate chiral amine. While (*R*)- and (*S*)-1-methylheptylamine are commercially available, (*R*)- and (*S*)-3,7-dimethyloctylamine were synthesised according to the procedure described by Koeckelberghs et al.[13] starting from commercially available (*R*)- and (*S*)-citronellol. Since a suitable chiral synthon is not commercial for the β-methyl-substituted amines, (*R*)- and (*S*)-2-methyloctylamine were synthesised from (*R*)- or (*S*)-2-octanol using an S_N2 reaction with cyanide after tosylation of the alcohol group. Some racemisation occurred during the S_N2 reaction which resulted in a decrease of the enantiomeric excess (*ee*) from 99% (as observed by chiral GC-FID) in (*R*)- or (*S*)-2-octanol to 60% in (*R*)- or (*S*)-2-cyano-octane (see Figure S1 in the Supporting Information). Since the reduction of 2-cyano-octane does not alter the *ee*, both *(R)*-2-methyloctylamine and (*S*)-2-methyloctylamine were isolated with *ee* values of 60%.

All aBTAs were obtained in high purity, as evidenced by MALDI-TOF-MS, elemental analysis and NMR. Since the optical purity of the amines employed was high, we can assume that the *ee* of all chiral aBTAs is $\geq$ 98.5%, except for aBTA-*R*/*S*-2Me showing *ee* values of 60%.

IR spectroscopy of BTAs in the solid state: IR spectroscopy is a sensitive tool to study the presence of intermolecular hydrogen bonding in BTAs in the solid state. Vibrations for the N–H stretch at $\approx$3240 cm^{-1}, the C=O stretch at $\approx$1640 cm^{-1} and the amide II at $\approx$1560 cm^{-1} have typically been attributed to the presence of threefold, α-helical-type intermolecular hydrogen bonding between neighbouring molecules.[7a,2a,g] We can now confirm, by measuring the IR spectrum of sBTA-methoxyethyl, which has a known crystal structure, that indeed these values are representative for well-defined intermolecular hydrogen bonds between neighbouring molecules within the same column (Table 1, entry 1; Figure S2A in the Supporting Information). In contrast, sBTA-CH_3 shows a completely deviating IR spectrum: two sharp N–H stretching vibrations are observed at 3333 and 3259 cm^{-1}, whereas the amide II band is found at the low value of 1539 cm^{-1} (Table 1, entry 2; Figure S2B in the Supporting Information). Indeed, in the crystal structure of sBTA-CH_3 no C_3 symmetry is present, but in contrast lateral hydrogen bonds are formed between the amides of molecules of different stacks.

All other aBTAs and sBTAs show IR vibrations at similar positions, although the N–H stretch vibration for sBTA-*S*-3Me is at the slightly lower value of 3223 cm^{-1} (Table 1, entries 3 and 5–11). As a typical example, the IR spectrum of aBTA-*S*-1Me is given in Figure 2A. Interestingly, in some BTAs, a different IR spectrum was measured after standing, which is indicative for a different crystal packing at room temperature (Figure S3 in the Supporting Information). For example, the IR spectrum of sBTA-C_8 can show an N–H stretch at the higher wavenumber of 3300 cm^{-1} and an amide II band at 1531 cm^{-1} (Table 1, entry 4). One can transform the latter crystal structure into the former by heating up the BTA to the isotropic melt and subsequently cooling it to room temperature. This effect was observed for sBTA-C_8, aBTA-*R*-3Me and aBTA-*S*-3Me, but not for the other aBTAs.

Table 1. Relevant IR vibrations for sBTAs and aBTAs.[a]

Entry	Compound	ν(N–H) [cm^{-1}]	ν(C=O) [cm^{-1}]	ν(amide II) [cm^{-1}]
1	sBTA-methoxyethyl	3250	1635	1551
2	sBTA-CH_3	3333/3259	1641	1539
3	sBTA-C_8H_{17}	3236	1640	1557
4	sBTA-C_8H_{17}[b]	3306	1644	1531
5	sBTA-*S*-3Me	3223	1637	1564
6	aBTA-*R*-1Me	3234	1634	1556
7	aBTA-*S*-1Me	3235	1635	1556
8	aBTA-*R*-2Me	3240	1638	1556
9	aBTA-*S*-2Me	3240	1637	1557
10	aBTA-*R*-3Me	3239	1636	1558
11	aBTA-*S*-3Me	3240	1639	1563

[a] All IR spectra were measured at room temperature. [b] IR vibrations of a different crystal structure.

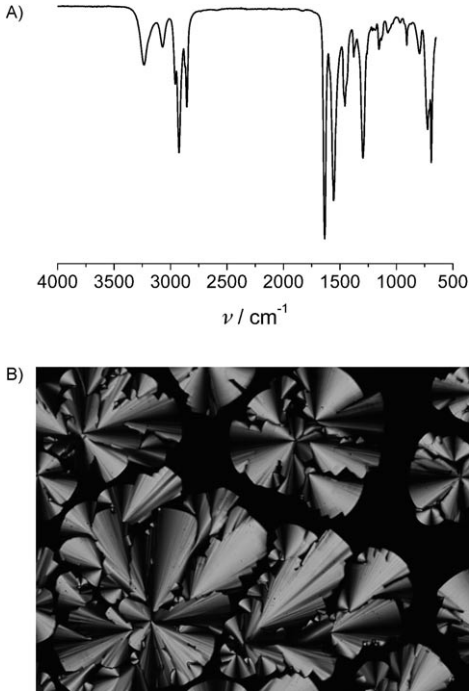

Figure 2. A) IR spectrum of aBTA-*S*-1Me. B) Optical texture of aBTA-*R*-1Me at 217°C (crossed polarizers) after slow cooling from the isotropic state.

Taking the IR results of sBTA-CH_3 into account, the deviating IR spectrum observed for sBTA-C_8, for example, must be related to the loss of the characteristic threefold intermolecular hydrogen-bonding motif in the solid state. Preliminary variable-temperature IR measurements show that for sBTA-C_8, for example, the C_3-symmetrical packing is not thermodynamically stable (Figure S4 in the Supporting Information). Although in the liquid-crystalline state C_3-symmetrical packing is dominant, upon cooling and standing for several days a rearrangement takes place. Presumably this is related to optimising space filling in the solid state.

Characterisation of the mesophase of the BTAs: With the help of POM and DSC, the thermal behaviour of the aBTAs was investigated. Under crossed polarisers, all asymmetric BTAs show birefringence at room temperature until the clearing temperature is reached. Slow cooling induces the growth of a pseudo-focal conic texture with large homeotropic areas (see Figure 2B) which is typical for a columnar hexagonal mesophase (Col_{ho}).

The melting temperatures (T_m) and clearing temperatures (T_{cl}) were determined by using DSC with heating rates of 10 K min^{-1}. All transition temperatures (in °C) and corresponding enthalpies (in kJ mol^{-1}) are collected in Table 2 and were derived from the second heating run. Although the thermal data for sBTA-C_8 (K 102 LC 204 I)[3a] and sBTA-*S*-3Me (K 119 Col 236 I)[7a] have been published before, we decided to remeasure them to have data available that are obtained under identical conditions.

Table 2. Transition temperatures [°C] and corresponding enthalpies [kJ mol^{-1}] of sBTAs and aBTAs obtained by DSC measurements.[a]

Compound	K	T (ΔH)	Col_{ho}	T (ΔH)
sBTA-C_8	●	19 (*17*)	●	198 (*8*)
sBTA-*S*-3Me	●	120 (*13*)	●	235 (*18*)
sBTA-*R*-3Me	●	120 (*9*)	●	233 (*13*)
aBTA-*R*-1Me	–	–	●	253 (*24*)
aBTA-*S*-1Me	–	–	●	255 (*27*)
aBTA-*R*-2Me	–	–	●	229 (*15*)
aBTA-*S*-2Me	–	–	●	226 (*18*)
aBTA-*R*-3Me	–	–	●	216 (*12*)
aBTA-*S*-3Me	–	–	●	211 (*13*)

[a] all DSC data are derived from the second heating run; ●: phase observed; –: phase not observed; K = crystalline phase; Col_{ho} = hexagonally ordered columnar phase; I = isotropic phase.

The melting temperature found for sBTA-C_8 in this study (K 19 M 198 I) is lower than that reported by Matsunaga et al. This can be explained by the fact that we determined the transition temperatures from the second heating run, whereas Matsunaga et al. derived their data from the first heating run.[3a] In fact, in the first heating, we also observe a broad melting peak at 119 °C. Presumably, these differences in melting temperatures are related to the different types of packing in the crystalline state (see discussion on the IR spectra above). In contrast, the transition temperatures for sBTA-*S*-3Me (K 120 M 235 I) are very similar to those previously reported.[7a]

Comparing the values of the transition temperatures T_m and T_{cl} of aBTAs shows an increase in the $Col_{ho} \rightarrow$ I transition (T_{cl}) when the chiral methyl group is closer to the amide group. Furthermore, T_{cl} is slightly lower in the asymmetrically substituted BTAs, as evidenced by comparing aBTA-*R*-3Me (T_{cl} = 216 °C) with sBTA-*R*-3Me (T_{cl} = 233 °C). The temperature range in which aBTA-3Me displays liquid crystallinity is much larger (over 300 K) than that of its symmetrical analogue (110 K). Cooling to −80 °C did not show crystallisation for the asymmetric BTAs in DSC conditions, but it is still possible that there is very slow crystallisation.

To date, BTAs have been widely studied by X-ray diffraction (XRD),[3a,b,5b] but, to the best of our knowledge, nobody has performed XRD experiments on aligned samples of BTAs in the liquid-crystalline state. XRD patterns of such aligned samples may confirm that the helical structure present in crystalline *N*,*N*′,*N*″-tris(2-methoxyethyl)benzene-1,3,5-tricarboxamide is retained in the liquid-crystalline state of analogous compounds. To confirm that the mesophase observed in all BTAs is indeed Col_{ho}, XRD measurements were performed on (aligned) samples of selected BTAs. The results are summarised in Table 3.

Table 3. Diffraction spacings in Å for BTAs.

hkl	aBTA-1Me[a,b]	aBTA-2Me[a,c]	aBTA-3Me[a,c]	sBTA-3Me[d,e]	sBTA-C_8[c]
1 0 0	15.8	16.0	16.3	17.2	16.0
1 1 0	9.1	9.3	9.5	9.9	9.1
2 0 0	8.0	8.1	8.2	8.6	8.1
halo	multiple	4.9	4.9	5.0	4.8
interdisc	3.4	3.5	3.5	3.5	3.5
intercolumn	18.2	18.5	18.9	19.9	18.5

[a] The *R* enantiomer was used. [b] Measurement at 180 °C. [c] Measurement at 159 °C. [d] Measurement at 140 °C. [e] Data from reference [15].

The diffraction pattern of a shear-aligned sample of sBTA-C_8 at 159 °C is given in Figure 3. Two features in the pattern allow the unambiguous assignment of a Col_{ho} phase. First, a set of three equatorial reflections in the small-angle region with spacings in the reciprocal ratio $1:\sqrt{3}:2$ is consistent with a hexagonal packing in the plane perpendicular to the shear direction. Second, a sharp arc is centred on the meridian and corresponds to 3.5 Å, which is the typical stacking distance in ordered columnar mesophases. Surprisingly, the diffuse halo that results from the aliphatic tails is not isotropic in this case. The azimuthal profile shows four distinct maxima that are about 45° off the meridian (Figure 3A). We propose two non-excluding hypotheses to explain this four split pattern (Figure 3B). First, the split can arise from a preferred conformation of the aliphatic tails tilted about 45° with respect to the column axis. This would improve the packing due to the low number of aliphatic tails to fill large spaces between the columns. Second, there is a periodicity of 6.9 Å along the column axis, corresponding to the q_z component of the scattering vector of these

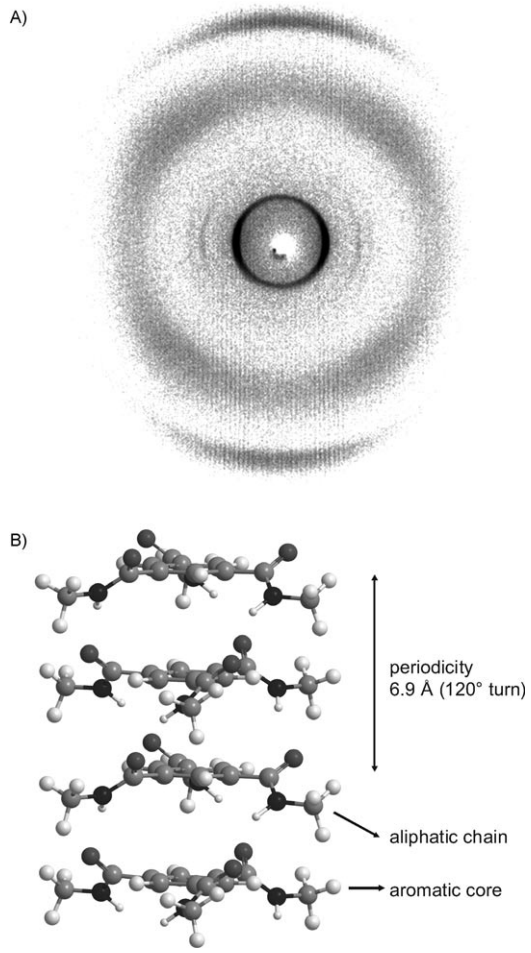

Figure 3. A) Diffraction pattern observed for aligned sBTA-C_8 measured at 159 °C. B) Model showing the proposed structure of a stack based on references [6a,b] and the characteristics of the structure, which can produce the splitting in the halo in the diffraction pattern.

maxima. This periodicity might be due to the helical structure of the stack and means that after two monomers (3.5 Å) we return to an equivalent position. Taking into account the C_3 symmetry of the molecules, there is a 60° turn between consecutive discs. This turn is the same as that described in the crystalline analogues[6] and allows for the threefold intermolecular hydrogen bonding, which gives rise to the threefold α helix. These two hypotheses are, however, not mutually exclusive, and it can be verified that the out-of-plane rotation of the amide groups to construct the intermolecular hydrogen bonds leads to a necessary tilt of about 45° of the alkyl tails with respect to the aromatic ring (Figure 3B).[6b] We thus think that the split in the halo due to the aliphatic tails proves that the helical structure in the liquid-crystalline phase is indeed the same as in the crystalline solids.

Unfortunately we could not achieve appropriate alignment of samples for the aBTAs. The powder patterns at high temperatures are, however, analogous to that of sBTA-C_8, which confirms a Col_{ho} phase for all aBTAs.[14] The intercolumnar distances found in the aBTAs and sBTAs are rather similar. Only sBTA-*R*-3Me shows a slightly larger intercolumnar spacing (19.9 Å), which can be rationalised by the three branched end groups at the aliphatic side chains.

Characterisation of aBTAs in solution with CD spectroscopy: To further characterise the stacking properties of the asymmetrically substituted BTAs, their self-assembly was investigated in dilute alkane solutions. In all cases, mirror-image CD spectra were obtained for enantiomer pairs (Figure S5 in the Supporting Information). Figure 4A shows the CD spectra of the aBTAs with the *R* configuration in methylcylcohexane (MCH) at a concentration of 30 μM; the corresponding molar ellipticities at $\lambda = 223$ nm are summarised in Table 4.

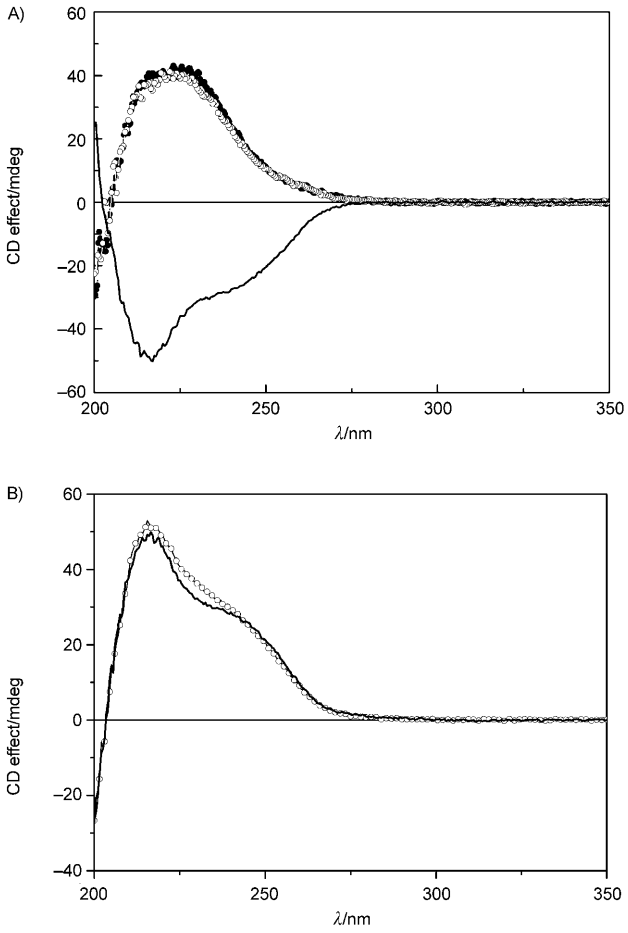

Figure 4. A) CD spectra of aBTA-*R*-1Me (●), aBTA-*R*-2Me (——) and aBTA-*R*-3Me (○) at a concentration of 30 μM in MCH at 20 °C. B) CD spectra of aBTA-*S*-2Me (——) at a concentration of 30 μM and aBTA-*S*-2MeBu (○) at a concentration of 140 μM in MCH at 20 °C.

The positive Cotton effects observed for the α- and γ-methyl-substituted aBTAs and the negative Cotton effect of the β-methyl-substituted aBTA indicate the presence of the odd–even effect. Whereas the shape and strength of the Cotton effect of aBTA-*R*-1Me ($\Delta\varepsilon = 41\ L\,mol^{-1}\,cm^{-1}$) and aBTA-*R*-3Me ($\Delta\varepsilon = 39\ L\,mol^{-1}\,cm^{-1}$) are almost identical, the shape of the Cotton effect of aBTA-*R*-2Me differs. The

Table 4. Molar ellipticities ($\Delta\varepsilon$) of aBTAs at $\lambda = 223$ nm in MCH at 20 °C and h_e values determined from CD cooling curves and from van 't Hoff plots.

Compound	$\Delta\varepsilon$ [L mol^{-1} cm^{-1}]	T_e[a] [K]	h_e (S.D.)[a] [kJ mol^{-1}]	h_e (R^2)[b] [kJ mol^{-1}]
aBTA-*R*-1Me	41	339.7	−59.7 (±0.8)	−69.4 (0.99)
aBTA-*S*-2Me	39	336.2	−55.6 (±0.7)	−69.8 (0.99)
aBTA-*R*-3Me	39	333.9	−59.8 (±0.6)	−68.6 (0.99)
aBTA-*S*-2MeBu	9	n.d.[c]	n.d.[c]	n.d.[c]
sBTA-*R*-3Me[d]	43	345.9	−60.9	−66.0
sBTA-C_8[e]	0	350.0	−69.6	−75.0

[a] Derived from the CD cooling curves, $c = 20$ μM in MCH, S.D. = standard deviation. [b] Derived from the van 't Hoff plot. [c] n.d. = not determined. [d] Data from reference [7b], $c = 21$ μM in heptane. [e] Data from reference [7b], $c = 22$ μM in heptane, data derived from UV measurements.

molar ellipticity at 223 nm ($\Delta\varepsilon = -39$ L mol^{-1} cm^{-1}), on the other hand, is similar in magnitude despite its lower enantiomeric excess (*ee*) value of 60%. Remarkably, the values for $\Delta\varepsilon$ of the aBTAs comprising only one chiral centre are close to the value of 43 L mol^{-1} cm^{-1} previously found for sBTA-*R*-3Me (Table 4), which has three chiral centra.[7b]

To rule out the possibility that the lower *ee* value is responsible for the different shape of the CD effect in the β-methyl-substituted aBTA, we prepared aBTA-*S*-2MeBu (Scheme 1) from (*S*)-2-methylbutylamine (*ee* > 99%). The shape of the CD spectra of both β-methyl-substituted aBTAs is similar (Figure 4B). However, the molar ellipticity of aBTA-*S*-2MeBu ($\Delta\varepsilon = 9$ L mol^{-1} cm^{-1} at 223 nm) is about four times smaller than that of aBTA-*S*-2Me ($\Delta\varepsilon = 39$ L mol^{-1} cm^{-1} at 223 nm). This large difference can be attributed to two different effects. First, there is low asymmetry around the chiral centre of aBTA-*S*-2MeBu and second, its chiral side chain is much shorter than the achiral side chains, resulting in a highly asymmetric system. The latter may result in poorer aggregation.

Stability of BTA stacks in MCH solution: The influence of the position of the methyl group on the stability of the aBTA aggregates in solution was investigated with temperature-dependent CD measurements at different concentrations in MCH. The temperature was decreased from 90 to 20 °C at $\lambda = 223$ nm because this is the maximum of the Cotton effect for aBTA-*R*-1Me and aBTA-*R*-3Me. The results are summarised in Figure 5; additional curves are given in Figure S5 in the Supporting Information.

As expected, the intensity of the CD effect decreases with decreasing concentration (Figure 5A).[7b] A typical temperature-dependent CD measurement at different concentrations is shown in Figure 5B. The curves in Figure 5B reveal two regimes; a nucleation regime, in which all molecules are molecularly dissolved (indicated by the absence of a CD effect) and an elongation regime in which the aggregate rapidly grows. Upon cooling, at a certain (concentration-dependent) temperature, the elongation temperature T_e, a large enough nucleus is formed to allow the formation of an aggregate. The increase in the degree of aggregation levels off

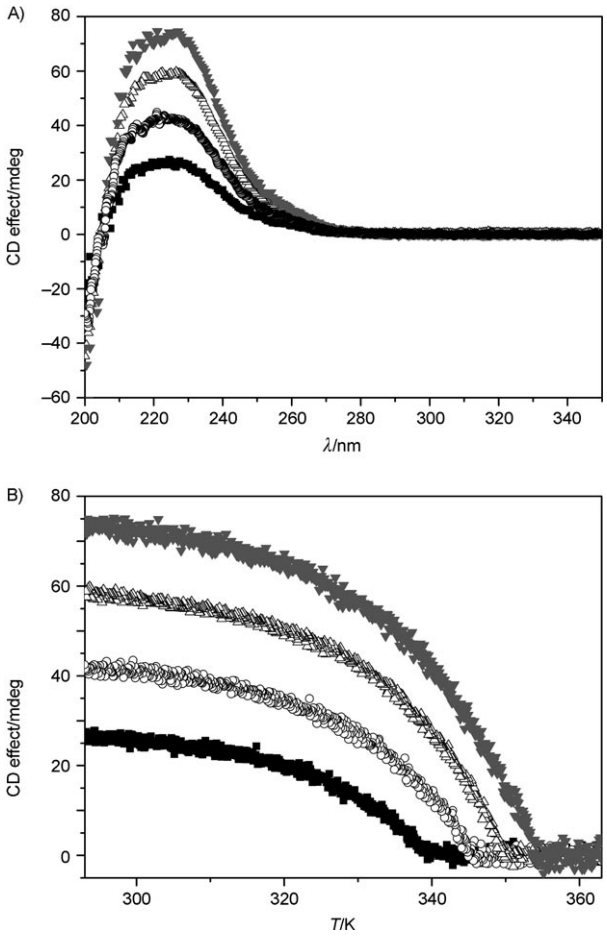

Figure 5. A) CD spectra of aBTA-*R*-1Me at 19 (■), 30 (○), 44 (△) and 49 μM (▽) at 20 °C. B) Results of the temperature-dependent CD measurements of aBTA-*R*-1Me at 19 (■), 30 (○), 44 (△) and 49 μM (▽) in MCH monitored at $\lambda = 223$ nm.

at around room temperature. Clearly, T_e increases with increasing concentration, indicative for the earlier (when cooling down from 90 °C) formation of aggregates.

Quantitative data on the self-assembly process can be derived from the CD cooling curves by fitting the data to a recently developed nucleation-growth model by van der Schoot,[16] which is a modified version of a model originally developed by Oosawa and Kasai.[17] We recently successfully used this model to describe the aggregation behavior of sBTA-*R*-3Me and sBTA-C_8.[7b] Fitting the cooling curves to the model affords T_e (the elongation temperature) and h_e (the enthalpy release upon elongation). Moreover, a dimensionless equilibrium constant K_a can be derived that reflects the degree of cooperativity in the aggregation process. The results of T_e and h_e as a function of the concentration are given in Figure 6 and the data for a 20 μM solution are shown in Table 4. All relevant thermodynamic data are collected in Table S5 in the Supporting Information.

Figure 6 and Table 4 show that aBTA-*R*-1Me has a slightly higher T_e than aBTA-*S*-2Me, which in turn has slightly higher T_e than aBTA-*R*-3Me, indicating that shifting the methyl moiety closer to the core gives a more stable aggre-

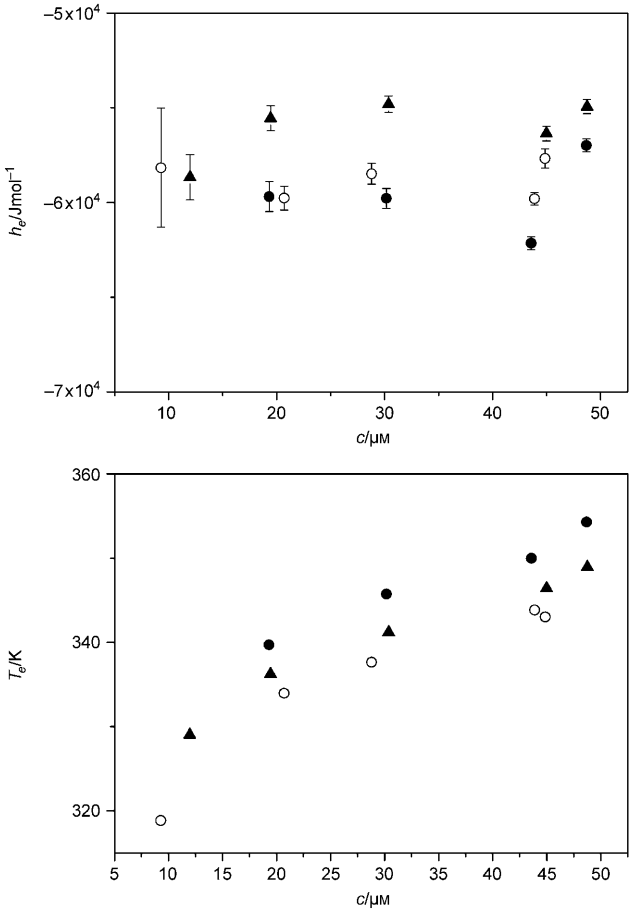

Figure 6. A) h_e as a function of concentration and B) T_e as a function of concentration, the standard deviations given for h_e result from the fit of the van der Schoot model. No standard deviations are displayed for the T_e because they are too small (typically ± 0.05 K). ●: aBTA-*R*-1Me, ○: aBTA-*R*-3Me and ▲: aBTA-*S*-2Me.

gate. The h_e values derived from the CD melting curves are between -55 and $-59\,kJ\,mol^{-1}$ and are concentration independent (Figure 6A). Interestingly, aBTA-*S*-2Me shows a slightly lower enthalpy release ($h_e = -55.6\,kJ\,mol^{-1}$) than the other aBTAs, which may be related to its lower *ee* value. All K_a values are very small ($=10^{-5}/10^{-6}$), indicating a highly cooperative system.

Fitting the natural logarithm of the (dimensionless) Cotton effect versus the reciprocal T_e allows for the construction of a modified van 't Hoff plot (Figure S6 in the Supporting Information), which provides a second method to determine the h_e value.[7b] The data are summarised in Table 4. The enthalpies obtained ($\approx -69\,kJ\,mol^{-1}$) are similar for all aBTAs and in between those previously reported for sBTA-*R*-3Me ($-66\,kJ\,mol^{-1}$) and sBTA-C_8 ($-75\,kJ\,mol^{-1}$).

Discussion

aBTAs show the presence of threefold, α-helical-type intermolecular hydrogen bonding between neighbouring molecules, as inferred from IR measurements in the solid state. In some cases, packing effects in the crystalline state result in a rearrangement of the hydrogen bonds, causing the loss of the characteristic threefold hydrogen-bonding motif. However, in the liquid-crystalline state, α-helical-type intermolecular hydrogen bonding is dominant. X-ray diffraction measurements confirm that all derivatives are in a Col_{ho} phase above T_m and that helical columnar order is preserved in the liquid-crystalline state. Moving the methyl group closer to the amide moiety, results in a stabilisation of the mesophase, as seen in the increase in T_{cl} from 216 to 253 °C and a concomitant increase in the transition enthalpies ΔH. Although there are small differences in the length of the chiral side chains, the observed differences in the T_{cl} are larger than expected based on the number of carbon atoms in the chiral side chain.

In dilute alkane solutions, the molar ellipticity ($\Delta\varepsilon$) of all aBTAs is around $\pm 40\,L\,mol^{-1}\,cm^{-1}$, which suggests that the degree to which the chirality of the side chain is transferred to the helical aggregate is independent of the position of the methyl group. This in contrast to induction of chirality in chiral polythiophenes and polyisocyanides; in these systems the Cotton effect decreases rapidly when the chiral substituent is placed further from the chromophore.[10a,11a,12] The stability of the aggregation process is affected by the position of the methyl group: T_e increases from 60.9 °C for the γ-methyl aBTA to 66.7 °C for the α-methyl aBTA. Unexpectedly, the position of the methyl group at an odd or an even position has a clear influence on the shape of the CD effect: in aBTA-*S*-2Me the CD spectrum shows a λ_{max} at 216 nm and a shoulder at 240 nm. As is clear from Figure 7, the spatial position of the methyl at an odd or even position is different with respect to its vicinity to the C=O group. This may inflict small changes in packing and hydrogen-bond lengths, which affect the shape of the CD spectra.

Conclusion

Asymmetrically substituted, chiral benzene-1,3,5-tricarboxamides are readily synthesised by coupling chiral amines to 3,5-bis-*n*-octylaminocarbonylbenzoic acid. In these aBTAs, the chiral methyl group varies in configuration (*R* or *S*) and position (α, β or γ) with respect to the amide group. IR spectroscopy revealed that in the solid state the aBTAs form columnar structures through threefold, α-helical-type intermolecular hydrogen bonding. All aBTAs are liquid crystalline at room temperature and with X-ray diffraction studies we could determine that the mesophase is Col_{ho} in all cases. Shifting the chiral methyl group in the aliphatic side chain closer to the amide bond stabilises the columnar structure as evidenced by an increase in the clearing temperature and enthalpy. In dilute solution, cooperative growth characterises the formation of aBTA aggregates, and moving the methyl group closer to the benzene core results in a more stable aggregate. A clear odd–even effect is present for aBTAs in dilute alkane solutions, and the degree to

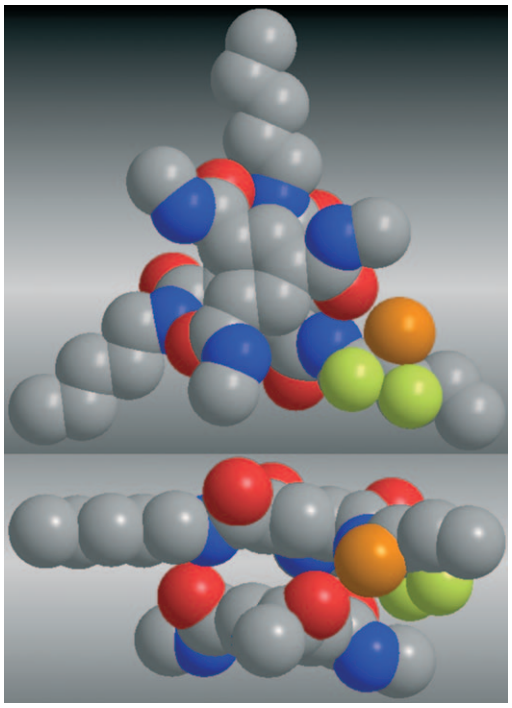

Figure 7. CPK models of aBTAs with a substituent at the 1 and 3 positions (*R* configuration) highlighted in yellow and at the 2 position (*S* configuration) highlighted in orange.

which the chirality of the side chain is transferred to the helical aggregate is independent of the position of the methyl.

Unexpectedly, we found that the shape of the CD effect differs when the methyl group is placed at an odd or an even position. The subtleties involved in the packing of aBTA-*R*/*S*-3Me, aBTA-*R*/*S*-2Me or aBTA-*R*/*S*-1Me are intriguing and currently we are performing vibrational CD (VCD) measurements on the aBTAs in solution to gather further information on packing effects. Moreover, we are performing sergeants-and-soldiers[18] and majority-rules experiments[19] to evaluate the impact of the position of the methyl group on the amplification of chirality in these systems. With this systematic study on the effect of the position of the chiral methyl goup in BTAs, we expect to increase our understanding of the subtleties involved in the self-assembly processes of seemingly simple compounds. Ultimately, our goal is to extend this understanding to achieve a design-driven, non-covalent synthesis of complex, functional supramolecular assemblies.

Experimental Section

Materials: (*S*)-Citronellol was obtained from Takasago, (98.4% *ee*), (*R*)-citronellol was obtained from Aldrich, 99% *ee*, (*S*)-2-octanol was obtained from Chiraselect (99.5% *ee*), (*R*)-2-octanol was obtained from Janssen Chimica (99% *ee*), (*S*)-2-octylamine was obtained from ABCR (99% *ee*, $[\alpha]_D^{23} = 6.16$, neat). (*R*)-2-octylamine was obtained from ABCR (99% *ee*, $[\alpha]_D^{23} = -5.99$, neat), (*S*)-2-methylbutanol was obtained from Acros ($[\alpha]_D^{23} = -5.80$, neat). 3,5-Bis(*n*-octylaminocarbonyl)benzoic acid was synthesised according to a previously published procedure.[5a] (*S*)-(−)-3,7-dimethyloctylamine, (*R*)-(+)-3,7-dimethyloctylamine and (*S*)-(−)-2-methylbutylamine[20] were synthesised following the procedures described by Koeckelberghs et al.[13] Reference compounds sBTA-CH_3[2a] and sBTA-methoxyethyl[6a] were prepared as described previously and recystallised from water and methanol, respectively. All solvents were obtained from Biosolve, except for DMSO (Acros) and spectrophotometric grade methylcylcohexane (Aldrich). All other chemicals were obtained from either Acros or Aldrich. Dry THF was tapped off a distillation setup which contained molecular sieves, $CHCl_3$ was dried over molsieves and triethylamine was stored on KOH pellets. All other chemicals were used as received.

Methods: UV/Vis and circular dichroism measurements were performed on a Jasco J-815 spectropolarimeter where the sensitivity, time constant and scan rate were chosen appropriately. Corresponding temperature-dependent measurements were performed with a PFD-425S/15 Peltier-type temperature controller with a temperature range of 263–383 K and adjustable temperature slope, in all cases a temperature slope of 1 K min^{-1} was used. In all other measurements the temperature was set at 20 °C. In all experiments the linear dichroism was also measured and in all cases no linear dichroism was observed. Separate UV/Vis spectra were obtained from a Perkin–Elmer UV/Vis spectrometer Lambda 40 at 20 °C. Cells with an optical path length of 1 cm were employed and spectroscopic grade solvents were employed. Solutions were prepared by weighing in the necessary amount of compound for a given concentration, whereafter this amount was transferred to a volumetric flask (flasks of 10, 25 and 50 mL were employed). Then the flask was filled for $^3/_4$ with the spectroscopic grade solvent and put in an oscillation bath at 40 °C for 45 min, whereafter the flask was allowed to cool down and filled up to its meniscus. The anisotropy value g was calculated from $\Delta\varepsilon$ and ε: $g = \Delta\varepsilon/\varepsilon$ and $\Delta\varepsilon$ = CD effect/(32980·c·l) in which c is the concentration in mol/L and l is the optical path length in cm. Optical rotations were recorded at room temperature on a Jasco DIP-370 polarimeter at a wavelength of 589 nm (NaD-line). ^{1}H and ^{13}C NMR spectroscopy measurements were conducted on a Varian Mercury 200 MHz and/or a Varian Gemini 400 MHz. Proton chemical shifts are reported in ppm downfield from tetramethylsilane (TMS). Carbon chemical shifts are reported using the resonance of $CDCl_3$ as internal standard. Maldi-TOF-MS were acquired using a Perserptive Biosystem Voyager-DE PRO spectrometer. In all cases, α-cyano-4-hydroxycinnamic acid was employed as the matrix material. Elemental analyses were performed on a Perkin–Elmer 2400 series II CHNS/O analyser. IR spectra were recorded on a Perkin–Elmer spectrum 1 using a universal ATR. Polarisation optical microscopy measurements were done using a Jenaval polarisation microscope equipped with a Linkam THMS 600 heating device, with crossed polarizers. The thermal transitions were determined with DSC using a Perkin–Elmer Pyris 1 DSC under a nitrogen atmosphere with heating and cooling rates of 10 K min^{-1}. The T_g was determined with heating and cooling rates of 40 K min^{-1}. The XRD patterns were obtained with a pinhole camera (Anton-Paar) operating with a point-focused Ni-filtered $Cu_{K\alpha}$ beam. In this setup, the samples are held in Lindemann glass capillaries (0.9 mm diameter). Aligned samples are obtained by shearing inside the capillary at the temperature of the mesophase, typically at 160 °C. The capillary axis is perpendicular to the X-ray beam and the pattern is collected on a flat photographic film perpendicular to the beam. Spacings are obtained via Bragg's law ($n\lambda = 2d\sin\theta$). The *ee* values of (*R*)- and (*S*)-2-cyano-octane were determined with GC-FID measurements using a Perkin–Elmer autosystem GC equipped with a WCOT fused silica column of 25 m × 0.25 mm with a CP Chirasel DEX CB DF = 0.12 coating. Separation of the enantiomers was performed under isothermal conditions with an oven temperature of 80 °C and a pressure of 11.6 or 12.0 psi. The *ee* values of commercially available (*R*)- and (*S*)-citronellol were measured on a Shimadzu GC-17A equipped with an FID detector and employing a Rt-βDex saTM column of Restek. Separation of the enantiomers was achieved using isothermal conditions with an oven temperature of 100 °C. In all cases, injection and detection temperatures were set at 250 °C.

Synthesis of *(S)*-(−)-2-methyloctylamine and *(R)*-(+)-2-methyloctylamine: A 100 mL three-necked round-bottom flask was charged with a solution of (*S*)-(+)-2-octanol (8.70 g, 0.0668 mol) in pyridine (20 mL), while keeping the solution at −5 °C in an ice/salt bath under an argon atmos-

phere. Subsequently, *p*-toluenesulfonyl chloride (1.1 equiv, 14.03 g, 0.0735 mol) was added to the mixture and the mixture was stirred overnight at 4 °C. After completion of the reaction was comfirmed by ^{1}H NMR spectroscopy, the excess *p*-toluenesulfonyl chloride was slowly quenched in small portions with cold H_2O. Subsequently, cold H_2O (100 mL) was added to the solution. This mixture was then extracted with $CHCl_3$ (3×100 mL), the organic layers were collected and washed with 1 M H_2SO_4 (3×100 mL) and 0.4 M $CuSO_4$ (3×100 mL) until no color change was observed in the copper sulfate, then the solution was washed once with H_2O. Drying of the organic layer with $MgSO_4$, filtration and concentration of the filtrate gave *(S)*-2-*p*-toluenesulfonate octane as a colorless oil (17.45 g, 92 %). ^{1}H NMR ($CDCl_3$): δ = 7.79 (d, 2H; Ar-*H*), 7.35 (d, 2H; Ar-*H*), 4.63 (sextett, 1H; O-C*H*), 2.45 (Ar-CH_3), 1.64–0.80 ppm (m, 16H; CH_2, CH_3). A 250 mL three-necked round-bottom flask was charged with a solution of (*S*)-2-*p*-toluenesulfonate octane (14.99 g, 0.052 mol) in DMSO (70 mL) under an argon atmosphere with a gas wash bottle filled with 1 M NaOH at the end of the gasflow. The mixture was heated to 50 °C. Subsequently, NaCN (1.1 equiv, 2.26 g, 0.057 mol) was added to the solution and the mixture was stirred overnight at 50 °C under an argon atmosphere. After the reaction was completed, the mixture was allowed to cool to room temperature, after which time it was transferred to a separating funnel and water (560 mL) was added. The water layer was extracted with CH_2Cl_2 (3×100 mL), the organic layers were collected and washed with 1 M KCl (3×100 mL). After evaporation in vacuo the crude product was obtained as a dark-brownish oil. Vacuum distillation afforded *(R)*-2-cyano-octane as a yellowish oil (4.46 g, 62 %, b.p. 56 °C at 0.27 mbar). ^{1}H NMR ($CDCl_3$): δ = 2.65–2.38 (m, 1H; CN-C*H*), 1.66–1.18 (m, 13H; CH_2, CH_3), 0.89 ppm (t, 3H; CH_3), trace amounts of 2-octanol; ^{13}C NMR ($CDCl_3$): δ = 123.0 (*C*≡N), 34.0 (*C*H_2), 31.5 (*C*H_2), 28.7 (*C*H_2), 26.9 (*C*H_2), 25.4 (*C*H), 22.4 (*C*H_2), 17.9 (*C*H_3), 13.9 ppm (*C*H_3), trace amounts of 2-octanol. A 250 mL three-necked round-bottom flask was charged with a solution of 1 M borane-THF-complex (60 mL) in dry THF (25 mL), while keeping the solution at 0 °C and under an argon atmosphere. A solution containing (*R*)-2-cyano-octane (4.00 g, 0.029 mol) in dry THF (25 mL) was slowly added to the reaction mixture through a dropping funnel. The mixture was stirred for 30 min at 0 °C, after which the mixture was heated at reflux for 1 h. Finally the mixture was stirred overnight at room temperature. After this, the mixture was cooled to 0 °C, and methanol (60 mL) was added dropwise (**CAUTION!** hydrogen gas is formed). Hydrochloric acid (37 % in water, 7 mL) was added slowly; the reaction mixture was stirred for 1 h and subsequently evaporated to dryness in vacuo. 2 M NaOH (100 mL) was added to the resulting viscous liquid and this was extracted with diethyl ether (3×200 mL). The organic layers were collected and dried with sodium sulfate, filtered and the solvent was removed in vacuo to obtain (*R*)-(+)-2-methyl-octylamine as a yellowish liquid (3.68 g, 88.6 %) ^{1}H NMR ($CDCl_3$): δ = 2.68–2.41 (m, 2H; NH_2-CH_2), 2.03 (s, 2H; NH_2), 1.62–1.15 (m, 11H; C*H*, CH_2), 0.96–0.85 ppm (m, 6H; CH_3), trace amounts of 2-octanol; $[\alpha]_D^{23}$ = 4.05 (neat). (*S*)-(−)-2-methyloctylamine was obtained in a similar fashion and obtained as a yellowish liquid (1.26 g, 80.0 %). ^{1}H NMR ($CDCl_3$): δ = 2.71–2.41 (m, 2H; NH_2-CH_2), 1.86 (s, 2H; NH_2), 1.62–1.17 (m, 11H; C*H*, CH_2), 1.00–0.86 ppm (m, 6H; CH_3), trace amounts of 2-octanol; $[\alpha]_D^{23}$ = −4.10 (neat).

General procedure for the synthesis of sBTAs: A 100 mL three-necked round-bottom flask was charged with a solution of the appropriated amine (62.2 mmol), triethylamine (1 equiv, 0.67 g, 66.2 mmol) in dry $CHCl_3$ (35 mL, stabilised with amylene) under inert atmosphere. A solution containing 1,3,5-benzenetricarboxylic acid chloride (0.3 equiv, 0.5 g, 18.8 mmol) in dry $CHCl_3$ (15 mL, stabilised with amylene) was slowly added dropwise to this solution. The solution was stirred overnight under inert atmosphere. The reaction mixture was then transferred to a separating funnel and washed with 1 M HCl (40 mL, check for acidity, pH < 1). The organic layer was collected and the solvent was removed in vacuo. The obtained crude product was then purified by recrystallisation from ethanol to obtain a white powder.

sBTA-C$_8$: sBTA-C_8 was obtained as a white solid (3.5 g, 54.9 %).^{1}H NMR ($CDCl_3$): δ = 8.34 (s, 3H; Ar-H), 6.56 (t, 3H; N-H), 3.47 (q, 6H; NH-CH_2), 1.68–1.28 (m, 36H; CH_2), 0.91 ppm (t, 9H; CH_3); ^{13}C NMR ($CDCl_3$): δ = 166.3 (*C*=O), 135.3 (Ar-*C*-C=O), 127.8 (Ar-*C*), 31.8 (NH-*C*), 29.5 (*C*H_2), 29.3 (*C*H_2), 29.2 (*C*H_2), 27.0 (*C*H_2), 22.6 (*C*H_2), 14.1 ppm (*C*H_3); IR: $\tilde{\nu}$ = 3236 (NH stretch), 1640 (C=O), 1557 cm^{-1} (amide II); MS (Maldi-TOF): *m/z*: 566.30 Da [*M*+Na$^+$]; elemental analysis calcd (%) for $C_{33}H_{57}N_3O_3$ (543.82 g mol^{-1}) C 72.88, H 10.56, N 7.73; found: C 72.77, H 10.90, N 7.45. observed DSC transitions: T_m = 19.8 °C, ΔH = 16.6 kJ mol^{-1}; T_{cl} = 198.4 °C, ΔH = 8.50 kJ mol^{-1}.

sBTA-S-*3Me*: sBTA-*S*-3Me was obtained as a white solid (0.77 g, 63 %).^{1}H NMR ($CDCl_3$): δ = 8.35 (s, 3H; Ar-*H*), 6.45 (t, 3H; N-*H*), 3.50 (m, 6H; NH-CH_2), 1.67–1.10 (m, 36H; C*H*, CH_2), 0.96 (d, 9H; CH_3), 0.88 ppm (d, 18H; 2×CH_3); IR: $\tilde{\nu}$ = 3223 (NH stretch), 1637 (C=O), 1564 cm^{-1} (amide II); MS (Maldi-TOF): *m/z*: 650.47 Da [*M*+Na$^+$]; elemental analysis calcd (%) for $C_{39}H_{69}N_3O_6$ (627.97 g mol^{-1}) C 74.59, H 11.07, N 6.69; found: C 74.01, H 10.94, N 6.63; observed DSC transitions: T_m = 119.7 °C, ΔH = 13.2 kJ mol^{-1}; T_{cl} = 234.9 °C, ΔH = 18.2 kJ mol^{-1}.

sBTA-R-*3Me*: sBTA-*R*-3Me was obtained as a white solid (0.39 g, 33 %). ^{1}H NMR ($CDCl_3$): δ = 8.34 (s, 3H; Ar-*H*), 6.40 (t, 3H; N-*H*), 3.49 (m, 6H; NH-CH_2), 1.69–1.14 (m, 36H; C*H*, CH_2), 0.95 (d, 9H; CH_3), 0.87 ppm (d, 18H; 2×CH_3). IR: $\tilde{\nu}$ = 3222 (NH stretch), 1637 (C=O), 1566 cm^{-1} (amide II); MS (Maldi-TOF): *m/z*: 650.48 Da [M+Na$^+$]; elemental analysis calcd (%) for $C_{39}H_{69}N_3O_6$ (627.97 g mol^{-1}): C 74.59, H 11.07, N 6.69; found: C 74.31, H 10.96, N 6.56; observed DSC transitions: T_m = 120.0 °C, ΔH = 9.3 kJ mol^{-1}; T_{cl} = 232.9 °C, ΔH = 12.9 kJ mol^{-1}.

General procedure for the synthesis of aBTAs: A 100 mL three-necked round-bottom flask was charged with a solution of 3,5-bis(*n*-octylaminocarbonyl)benzoic acid (0.220 g, 0.509 mmol), DMAP (1.7 equiv, 0.106 g) and the appropriated amine (1.7 equiv, 0.865 mmol)[21] in dry $CHCl_3$ (30 mL) under an argon atmosphere; the solution was cooled in an ice/salt bath. A solution containing 1-(3-dimethylpropyl)-3-ethylcarbodiimide hydrochloride (EDC; 1.7 equiv, 0.162 g, 0.865 mmol) in dry $CHCl_3$ (10 mL) was quickly added to the reaction mixture. The solution was stirred for 4 d under an argon atmosphere. The mixture was then transferred to a separating funnel and $CHCl_3$ (50 mL) was added and subsequently washed with 1 M HCl (50 mL), 10 % aqueous $NaHCO_3$ (50 mL) and brine (50 mL). The solvent was removed in vacuo before the crude product was purified by means of column chromatography. Column chromatography was performed by using silica gel (9 g) in a column with a diameter of 1.5 cm; the silica was equilibrated in $CHCl_3$. Because of the relatively poor solubility of the crude product in chloroform, the crude product was dissolved in a large volume of chloroform, silica gel was added (around 1 g), the mixture was stirred for 15 min and was evaporated to dryness in vacuo. This impregnated silica was then poured on top of the column. The eluent was then applied (chloroform/ethyl acetate 8:2 v/v) and the product fractions were collected (monitored by TLC) and the solvent was removed in vacuo to obtain a white solid.

aBTA-S-*3Me*: aBTA-*S*-3Me was obtained as a sticky white solid (0.1634 g, 56 %). ^{1}H NMR ($CDCl_3$): δ = 8.34 (s, 3H; Ar-*H*), 6.41 (t, 3H; N-*H*), 3.50 (m, 6H; NH-CH_2), 1.72–1.13 (m, 36H; C*H*, CH_2), 0.96 −0.85 ppm (m, 15H; CH_3); IR: $\tilde{\nu}$ = 3240 (NH stretch), 1639 (C=O), 1563 cm^{-1} (amide II); MS (Maldi-TOF): *m/z*: 594.50 [*M*+Na$^+$]; observed DSC transitions: T_{cl} = 211.2 °C, ΔH = 12.8 kJ mol^{-1}.

aBTA-R-*3Me*: aBTA-*R*-3Me was obtained as a sticky white solid (0.0904 g, 68.7 %). ^{1}H NMR ($CDCl_3$): δ = 8.33 (s, 3H; Ar-*H*), 6.55 (t, 3H; N-*H*), 3.45 (m, 6H; NH-CH_2), 1.73–1.14 (m, 31H; C*H*, CH_2), 0.94–0.83 ppm (m, 15H; CH_3); IR: $\tilde{\nu}$ = 3239 (NH stretch), 1636 (C=O), 1558 cm^{-1} (amide II); MS (Maldi-TOF): *m/z*: 594.36 [*M*+Na$^+$]; observed DSC transitions: T_{cl} = 215.9 °C, ΔH = 11.8 kJ mol^{-1}.

aBTA-R-*2Me*: aBTA-*R*-2Me was obtained as a sticky white solid (0.1363 g, 48 %). ^{1}H NMR ($CDCl_3$): δ = 8.38 (s, 3H; Ar-*H*), 6.43 (t, 3H; N-*H*), 3.55–3.27 (m, 6H; NH-CH_2), 1.73–1.16 (m, 31H; C*H*, CH_2), 1.02–0.84 ppm (m, 15H; CH_3); IR: $\tilde{\nu}$ = 3240 (NH stretch), 1638 (C=O), 1556 cm^{-1} (amide II); MS (Maldi-TOF): *m/z*: 558.36 Da [*M*+H$^+$]; observed DSC transitions: T_{cl} = 229.2 °C, ΔH = 14.9 kJ mol^{-1}.

aBTA-S-*2Me*: aBTA-*S*-2Me was obtained as a sticky white solid (0.1326 g, 47 %). ^{1}H NMR ($CDCl_3$): δ = 8.34 (s, 3H; Ar-*H*), 6.48 (t, 3H; N-*H*), 3.50–3.27 (m, 6H; NH-CH_2), 1.75–1.14 (m, 35H; C*H*, CH_2), 1.00–0.84 ppm (m, 12H; CH_3); IR: $\tilde{\nu}$ = 3240 (NH stretch), 1637 (C=O), 1557 cm^{-1} (amide II); MS (Maldi-TOF): *m/z*: 580.34 Da [*M*+Na$^+$]; observed DSC transitions: T_{cl} = 226.0 °C, ΔH = 18.4 kJ mol^{-1}.

aBTA-R-*1Me*: aBTA-*R*-1Me was obtained as a sticky white solid (0.1761 g, 46%). ^{1}H NMR ($CDCl_3$): $\delta = 8.25$ (s, 3H; Ar-*H*), 6.80 (t, 2H; N-*H*), 6.47 (d, 1H; N-*H*), 4.16 (sextett, 1H; NH-C*H*), 3.45 (q, 4H; NH-CH_2), 1.68–1.17 (m, 36H; CH_2), 0.88 ppm (t, 9H; CH_3); IR: $\tilde{\nu} = 3234$ (NH stretch), 1634 (C=O), 1556 cm^{-1} (amide II); MS (Maldi-TOF): *m*/*z*: 566.33 Da [*M*+Na$^+$]; elemental analysis calcd (%) for $C_{33}H_{57}N_3O_3$ (543.82 g mol^{-1}): C 72.88, H 10.56, N 7.73; found: C 72.75, H 10.45, N 7.74; observed DSC transitions: $T_{cl} = 252.9$ °C, $\Delta H = 24.1$ kJ mol^{-1}.

aBTA-S-*1Me*: aBTA-*S*-1Me was obtained as a sticky white solid (0.1828 g, 48%). ^{1}H NMR ($CDCl_3$): $\delta = 8.25$ (s, 3H; Ar-*H*), 6.77 (t, 2H; N-*H*), 6.47 (d, 1H; N-*H*), 4.16 (sextett, 1H; NH-C*H*), 3.45 (q, 4H; NH-CH_2), 1.66–1.16 (m, 36H; CH_2), 0.90 ppm (t, 9H; CH_3); IR: $\tilde{\nu} = 3235$ (NH stretch), 1635 (C=O), 1556 cm^{-1} (amide II); MS (Maldi-TOF): *m*/*z*: 566.38 Da [*M*+Na$^+$]; elemental analysis calcd (%) for $C_{33}H_{57}N_3O_3$ (543.82 g mol^{-1}): C 72.88, H 10.56, N 7.73; found: C 72.43, H 10.43, N 7.73; observed DSC transitions: $T_{cl} = 255.0$ °C, $\Delta H = 26.5$ kJ mol^{-1}.

aBTA-S-*2MeBu*: aBTA-*S*-2MeBu was obtained as a sticky white solid (0.070 g, 60%). ^{1}H NMR ($CDCl_3$): $\delta = 8.30$ (s, 3H; Ar-*H*), 6.41 (t, 3H; N-*H*), 3.44–3.22 (m, 6H; NH-CH_2), 1.60–1.15 (m, 27H; C*H*, CH_2), 0.94–0.77 ppm (m, 12H; CH_3). IR: $\tilde{\nu} = 3239$ (NH stretch), 1639 (C=O), 1558 cm^{-1} (amide II); MS (Maldi-TOF): *m*/*z*: 524.47 Da [*M*+Na$^+$]; observed DSC transitions: $T_{cl} = 222.6$ °C,[22] $\Delta H = 2.2$ kJ mol^{-1}.

Acknowledgements

The authors would like to thank Dr. J. A. J. M. Vekemans for stimulating discussions, Martijn Gillissen, Fokko Haveman and Dirk Balkenende for their help with the synthesis and the NRSC-C and NWO for financial support. R.M.-R. acknowledges support from an EU Marie Curie Intra-European Fellowship (Project MEIF-CT-2006-042044) within the EC Sixth Framework Program. We gratefully thank Dr. J. Barberá for providing us access to the powder X-ray diffraction equipment at the University of Zaragoza (ES) and Philips Research in Eindhoven (NL) for allowing us access to the X-ray facilities.

[1] a) G. M. Whitesides, E. E. Simanek, J. P. Mathias, C. T. Seto, D. Chin, M. Mammen, D. M. Gordon, *Acc. Chem. Res.* **1995**, *28*, 37–44; b) S. J. Rowan, S. J. Cantrill, G. R. L. Cousins, J. K. M. Sanders, J. F. Stoddart, *Angew. Chem.* **2002**, *114*, 898–952; *Angew. Chem. Int. Ed.* **2002**, *41*, 938; c) F. J. M. Hoeben, P. Jonkheijm, E. W. Meijer, A. P. H. J. Schenning, *Chem. Rev.* **2005**, *105*, 1491–1546; d) A. J. Wilson, *Soft Matter* **2007**, *3*, 409–425; e) R. V. Ulijn, A. M. Smith, *Chem. Soc. Rev.* **2008**, *37*, 664–675; f) D. M. Vriezema, M. C. Aragones, J. A. A. W. Elemans, J. J. L. M. Cornelissen, A. E. Rowan, R. J. M. Nolte, *Chem. Rev.* **2005**, *105*, 1445–1489.

[2] a) K. Hanabusa, C. Koto, M. Kimura, H. Shirai, A. Kakehi, *Chem. Lett.* **1997**, *5*, 429–430; b) Y. Yasuda, E. Iishi, H. Inada, Y. Shirota, *Chem. Lett.* **1996**, *7*, 575–576; c) S. J. Lee, C. R. Park, J. Y. Chang, *Langmuir* **2004**, *20*, 9513–9519; d) A. Sakamoto, D. Ogata, T. Shikata, K. Hanabusa, *Macromolecules* **2005**, *38*, 8983–8986; e) T. Shikata, D. Ogata, K. Hanabusa, *J. Phys. Chem. B* **2004**, *108*, 508–514; f) A. Sakamoto, D. Ogata, T. Shikata, O. Urakawa, K. Hanabusa, *Polymer* **2006**, *47*, 956–960; g) D. Ogata, T. Shikata, K. Hanabusa, *J. Phys. Chem. B* **2004**, *108*, 15503–15510; h) A. R. A. Palmans, J. A. J. M. Vekemans, R. A. Hikmet, H. Fischer, E. W. Meijer, *Adv. Mater.* **1998**, *10*, 873–876; i) M. de Loos, J. H. van Esch, R. M. Kellogg, B. L. Feringa, *Tetrahedron* **2007**, *63*, 7285–7301.

[3] a) Y. Matsunaga, Y. Nakayasu, S. Sakai, M. Yonenaga, *Mol. Cryst. Liq. Cryst.* **1986**, *141*, 327–333; b) Y. Matsunaga, N. Miyajima, Y. Nakayasu, S. Sakai, M. Yonenaga, *Bull. Chem. Soc. Jpn.* **1988**, *61*, 207–210; c) A. R. A. Palmans, J. A. J. M. Vekemans, H. Fischer, R. A. Hikmet, E. W. Meijer, *Chem. Eur. J.* **1997**, *3*, 300–307; d) J. J. van Gorp, J. A. J. M. Vekemans, E. W. Meijer, *J. Am. Chem. Soc.* **2002**, *124*, 14759–14769; e) K. P. van den Hout, R. Martín-Rapún, J. A. J. M. Vekemans, E. W. Meijer, *Chemistry* **2007**, *13*, 8111–8124.

[4] a) M. Blomenhofer, S. Ganzleben, D. Hanft, H.-W. Schmidt, M. Kristiansen, P. Smith, K. Stoll, D. Maeder, K. Hoffmann, *Macromolecules* **2005**, *38*, 3688–3695; b) N. Mohmeyer, N. Behrendt, X. Zhang, P. Smith, V. Altstädt, G. M. Sessler, H.-W. Schmidt, *Polymer* **2007**, *48*, 1612–1619.

[5] a) J. Roosma, T. Mes, P. Leclère, A. R. A. Palmans, E. W. Meijer, *J. Am. Chem. Soc.* **2008**, *130*, 1120–1121; b) C. F. C. Fitié, I. Tomatsu, D. Byelov, W. H. de Jeu, R. P. Sijbesma, *Chem. Mater.* **2008**, *20*, 2394–2404.

[6] a) M. P. Lightfoot, F. S. Mair, R. G. Pritchard, J. E. Warren, *Chem. Commun.* **1999**, 1945–1946; b) P. P. Bose, M. G. B. Drew, A. K. Das, A. Banerjee, *Chem. Commun.* **2006**, 3196–3198.

[7] a) L. Brunsveld, A. P. H. J. Schenning, M. A. C. Broeren, H. M. Janssen, J. A. J. M. Vekemans, E. W. Meijer, *Chem. Lett.* **2000**, *3*, 292–293; b) M. M. J. Smulders, A. P. H. J. Schenning, E. W. Meijer, *J. Am. Chem. Soc.* **2008**, *130*, 606–611.

[8] The solubility of *N*,*N*′,*N*″-tris((*S*)-1-methylheptyl)benzene-1,3,5-tricarboxamide and *N*,*N*′,*N*″-tris((*R*)-1-methylheptyl)benzene-1,3,5-tricarboxamide was below 10^{-6} M in MCH.

[9] a) W. H. de Jeu, J. van der Veen, *Mol. Cryst. Liq. Cryst.* **1977**, *40*, 1–17; b) G. W. Gray, D. G. McDonnel, *Mol. Cryst. Liq. Cryst.* **1977**, *34*, 211–217; c) D. Demus in *Handbook of Liquid Crystals Volume 1: Fundamentals* (Eds.: D. Demus, J. Goodby, G. W. Gray, H.-W. Spiess, V. Vill), Wiley-VCH, Weinheim **1998**, Chapter VI, pp. 146–152; d) J. W. Goodby in *Handbook of Liquid Crystals Volume 1: Fundamentals* (Eds.: D. Demus, J. Goodby, G. W. Gray, H.-W. Spiess, V. Vill), Wiley-VCH, Weinheim **1998**, Chapter V, pp. 124–126.

[10] a) D. B. Amabilino, J.-L. Serrano, T. Sierra, J. Veciana, *J. Pol. Sci. Part A: Polym. Chem.* **2006**, *44*, 3161–3174; b) H. Nakashima, J. R. Koe, K. Torimitsu, M. Fujiki, *J. Am. Chem. Soc.* **2001**,*123*, 4847–4848; c) J. Zhi, Z. Zhu, A. Liu, J. Cui, X. Wan, Q. Zhou, *Macromolecules* **2008**, *41*, 1594–1597.

[11] a) E. R. Lermo, B. Langeveld-Voss, R. A. J. Janssen, E. W. Meijer, *Chem. Commun.* **1999**, 791–792; b) O. Henze, W. J. Feast, F. Gardebien, P. Jonkheijm, R. Lazzaroni, P. Leclère, E. W. Meijer, A. P. H. J. Schenning, *J. Am. Chem. Soc.* **2006**, *128*, 5923–5929.

[12] D. B. Amabilino, E. Ramos, J.-L. Serrano, T. Sierra, J. Veciana, *J. Am. Chem. Soc.* **1998**, *120*, 9126–9134.

[13] G. Koeckelberghs, L. De Cremer, W. Vanormelingen, W. Dehaen, T. Verbiest, A. Persoons, C. Samyna, *Tetrahedron* **2005**, *61*, 687–691.

[14] The pattern at RT is not characteristic of a liquid-crystalline phase due to the appearance of a series of discrete maxima in place of the diffuse halo due to the aliphatic chains, although no transition was detected either by DSC or by POM.

[15] P. J. M. Stals, J. F. Haveman, R. Martín-Rapún, C. F. C. Fitié, A. R. A. Palmans, E. W. Meijer, *J. Mater. Chem.* **2009**, *19*, 124–130.

[16] a) P. van der Schoot in *Supramolecular Polymers* (Ed.: A. Cifferi), Taylor & Francis, London, **2005**; b) P. Jonkheijm, P. van der Schoot, A. P. J. H. Schenning, E. W. Meijer, *Science* **2006**, *313*, 80–83.

[17] F. Oosawa, M. Kasai, *J. Mol. Biol.* **1962**, *4*, 10–21.

[18] M. M. Green, M. P. Reidy, R. D. Johnson, G. Darling, D. J. O'Leary, G. Willson, *J. Am. Chem. Soc.* **1989**, *111*, 6452–6454.

[19] M. M. Green, B. A. Garetz, B. Munoz, H. Chang, S. Hoke, R. G. Cooks, *J. Am. Chem. Soc.* **1995**, *117*, 4181–4182.

[20] Since 2-methylbutylamine had a very low boiling point, it was necessary to transform it into a salt by adding CF_3COOH (1.2 equiv) to the organic layers just before the removal of diethyl ether and removing the surplus of CF_3COOH and the diethyl ether in vacuo.

[21] In the case of aBTA-*S*-2MeBu, TEA (2 equiv) was also added to reaction mixture. This was needed to deprotonate the trifluoroacetic acid-amine salt to obtain (*S*)-2-methylbutylamine.

[22] As observed in the first heating run at 40 K min^{-1}. No transitions were observed in the second and consecutive runs.

Received: October 23, 2008
Published online: January 13, 2009

